

Mesoscopic Transport and Interferometry with Wavepackets of Ultracold atoms: Effects of Quantum Coherence and Interactions

Kunal K. Das

Department of Physical Sciences, Kutztown University of Pennsylvania, Kutztown, Pennsylvania 19530, USA

(Dated: January 12, 2021)

We propose a way to simulate mesoscopic transport processes with counter-propagating wavepackets of ultracold atoms in quasi one-dimensional (1D) waveguides, and show quantitative agreement with analytical results. The method allows the study of a broad range of transport processes at the level of *individual modes*, not possible in electronic systems. Typically suppressed effects of quantum coherence become manifest, along with the effects of tunable interactions, which can be used to develop a simpler type of sensitive atom interferometer.

PACS numbers: 05.60.Gg, 73.23.-b, 03.75.Dg, 67.85.-d

Atomtronics, or electronics with ultracold atoms, is an emerging field with broad potential. Exploratory papers on the subject have focussed on atomic replicas of electronic components like transistors [1–3]. The degenerate temperatures and the quantum nature of ultracold atoms however, makes atomtronics akin to nanoscale mesoscopic processes [4], rather than traditional electronics. Therefore, besides component design, progress in atomtronics calls for the study and simulation of the transport mechanisms by which mesoscopic circuits operate.

Fermionic atoms in waveguides can mimic electrons in nanowires [5]. But it is the possibility of bosonic carriers that makes atomtronics more than an imitation of mesoscopic electronics. Carrier statistics can influence the characteristics of atomtronics components [3], although not their functionality. But in atomtronics implementations of mesoscopic transport, bosons can offer significant advantages by bypassing certain assumptions implicit in the solid state such as: (i) multiple modes always present with fermionic carriers, that suppress coherent correlations and (ii) fixed inter-particle interactions, often ignored in models of ballistic transport in nanowires [4].

Transport experiments with degenerate bosons require a different approach, since there is no exclusion principle to guarantee non-vanishing momenta essential for fermionic transport processes. We therefore propose to simulate the basic Landauer [4, 6] paradigm of mesoscopic transport with wavepackets of cold bosons, which allows an enhanced flexibility of operation that brings out features absent or suppressed in electronic transport.

Mesoscopic Transport with wavepackets: In mesoscopic solid state systems transport is described by quantum scattering [4, 6]. Fermionic carriers move ballistically in quasi 1D nanoscale leads between macroscopic contacts that act as absorbing reservoirs for the carriers. Any device connected to the wire acts as a scatterer. In a single-channel circuit with two leads (left $\rightarrow l$, right $\rightarrow r$), the particle current for spin-polarized fermions (F),

$$J_F = \int_0^\infty \frac{dk}{2\pi} [v(k)f_l(k)T_l(k) - v(k)f_r(k)T_r(k)], \quad (1)$$

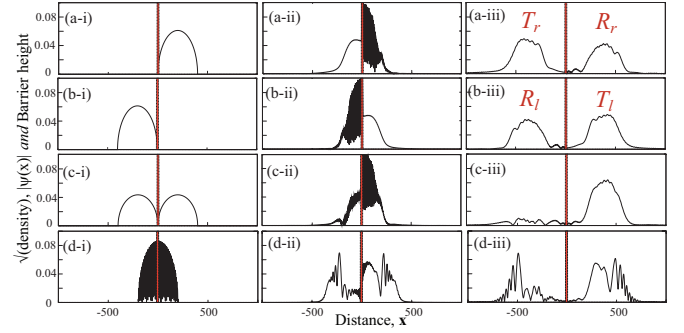


FIG. 1: Simulation of mesoscopic transport with wavepackets of Thomas-Fermi profile $|\psi(x, 0^-)| = \sqrt{b^2 - (x - x_0)^2}$, $b = 200$ and velocity $k = 0.5$, for a static rectangular barrier slightly shifted from the origin: (a) Left incident packet, (b) Right incident packet, (c) Simultaneous left and right incident packets propagating coherently, and (d) Single wavepacket split into 50-50 superposition of $\pm\hbar k$ momentum states, similar to (c) but with additionally two outbound fractions.

is determined by the Fermi distribution functions $f_{l(r)}$ of the contacts, the transmission probabilities $T_{l(r)}$ for left and right incident particles and their velocities $v(k)$. The underlying picture is that of carriers injected at all available modes k in both leads and the net current is given by the weighted sum of the current at *each mode*,

$$J_B(k) = \frac{v}{2} [(f_l - f_r) + (f_l T_l + f_r R_r) - (f_l R_l + f_r T_r)], \quad (2)$$

termed bosonic (B) being single mode, in contrast with multi-mode fermionic currents. The first term is due to inbound particles, bias driven with no scatterer. The last two terms are *incoherent* sums of the reflected and transmitted fractions, outbound from the scatterer.

The single mode current is determined by the scattering probabilities, therefore it can be directly simulated with ultracold atoms: Start with a wavepacket $\psi(x, t = 0^-)$ of ultracold atoms (of axial extent $2b$) in a quasi-1D harmonic trap [5], first on the left and then on the right of the “device” (a scattering potential implemented with tightly focussed lasers, blue or red de-

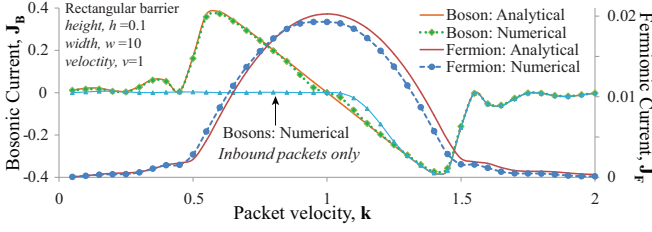


FIG. 2: Wavepacket simulation with a single split wavepacket as in Fig. 1(d), compared to exact analytical [5] current profile of a ‘snowplow’ quantum pump operating by a translating potential. Fermionic and Bosonic currents are plotted. Inbound packets alone [Fig. 1(c)] are insufficient for $k < v$. Numerical curves are interpolations of the marked computed values.

tuned for barriers or wells). To initiate the transport experiment, at $t = 0$ the axial trap is turned off and the atoms given an inward momentum $\pm \hbar k$ by using Bragg beams [7], $\psi(x, 0^+) = e^{\pm i k x} \psi(x, 0^-)$. The wavepacket is allowed to evolve for $t_f > 2kb$ such that the scattered wavepacket has little overlap with the device, and then the spatial and momentum distribution imaged. The integrated densities $n_{\pm}(t_f) = \int dk \theta(\pm k) |\psi(k, t_f)|^2$ of the left(-) and right(+) moving scattered fractions directly give the scattering probabilities; which, for broad packets, match those of plane waves $e^{\pm i k x}$. Along with $f_{l(r)}$ of the system, they determine $J_B(k)$. Snapshots of the propagation of the spatial wavefunction with a split-step operator method are shown in Fig. 1(a,b). Fermionic transport is simulated by replacing the integral in Eq. (1) by a Riemann sum sampled at discrete intervals of Δk :

$$J_F = \int_{-\infty}^{\infty} \frac{dk}{2\pi} f(k) J_B(k) \simeq \frac{\Delta k}{2\pi} \sum_i f(k_i) J_B(k_i). \quad (3)$$

Figure 2 shows the accuracy of this approach for both single mode bosonic transport and integrated fermionic transport for a ‘snowplow’ quantum pump [5] of interest in mesoscopic physics. The key point is that J_B needs to be sampled only at some points in k -space to map out J_F .

The power of the method is in its simplicity and the variations it allows for exploring transport features, many not possible in mesoscopic systems: (i) Nonlinear transport, tunable by Feshbach resonances [8] in packets of BEC in an optical dipole trap [9]; (ii) quantum to semiclassical limit by narrowing packet widths; (iii) transport and resonance transmission with different potentials by sculpting laser profiles and bias fields; (iv) time-varying potentials; (v) coherence effects by propagating left and right going packets simultaneously [Fig. 1(c)]; (vi) adjustable periodic potential with optical lattices.

Simulation and Physical Parameters: To describe coherent superpositions and velocity-changing time-varying scatterers, Eq. (2) is generalized to

$$J[\psi(k, t)] = (\hbar/m) \langle \psi(k, t) | k | \psi(k, t) \rangle / \langle \psi(k, t) | \psi(k, t) \rangle. \quad (4)$$

This, at $t = t_f$ after scattering, corresponds to the last two terms of Eq. (2); the first term determined by the Fermi functions, vanishes for biasless transport $f_l = f_r$. Possible initial states in position space $\psi(x, 0^-)$ are shown in Fig. 1. For incoherent sum of left [Fig. 1(a)] and right going [Fig. 1(b)] packets, the currents are computed separately and averaged $J = \frac{1}{2}[J[\psi_l(k, t)] + J[\psi_r(k, t)]]$. Packets are weighted by $f_{l(r)}$ for biased transport.

Assuming degenerate bosons, we use initial Thomas-Fermi profile $|\psi(x, 0^-)|^2 = b^2 - (x - x_0)^2$. The packet(s) are propagated with the 1D Gross-Pitaevskii (GP) equation $[-\frac{\hbar^2}{2m} \partial_x^2 + V(x) + g_{1D} |\psi|^2] \psi = -i \hbar \partial_t \psi$, the nonlinearity [10] measured by the effective 1D interaction $g_{1D} = 2aN$ ($a \rightarrow$ scattering length, $N \rightarrow$ number of atoms). The transverse trap frequency ω_r defines our units $l = \sqrt{\hbar/(m\omega_r)}$, $E_0 = \hbar\omega_r$ and $\tau = \omega_r^{-1}$. In the non-interacting case $g_{1D} = 0$, but the Thomas-Fermi profile is still used, as results are insensitive to packet shape, if wide enough to approximate plane waves [Fig. 6]. Also, a small nonlinearity $g_{1D} \simeq 1$ can substantially broaden the initial packet and still approximate linear behavior.

Any atom species with a BEC and a Feshbach resonance through zero scattering length may be used. For example, with ^{39}K in a trap of radial and axial frequencies of $\omega_r = 2\pi \times 600$ Hz and $\omega_a = 2\pi \times 0.6$ Hz, possible in current experiments [11], our units are $l = 0.65 \mu\text{m}$, $E_0 = 0.029 \mu\text{K}$ and $\tau = 0.26$ ms. With scattering length tuned to $0.05a_B$, in these units $g_{1D} = 0.81$ and packet width $b = 106$ for $N = 10^5$ atoms [12], appropriate for testing linear transport. A scattering length of $1.5a_B$ gives $g_{1D} = 24$ and $b = 330$, sufficient to test nonlinear transport described here. Our simulations use wider packets $b = 600$ only for precise matching of plane wave results [Fig. 6]. Typical packet velocity $l/\tau = 2.5 \text{ mm/s}$ defines the time scale of experiments, $2kb \simeq 50$ ms.

Transport Interferometry with Static Potentials: Mesoscopic transport assumes lack of phase coherence among individual carriers, due to the randomization in the reservoirs [4]; hence the *incoherent* sum of transmission probabilities in Eq. (1). With trapped atoms we can relax this condition with some interesting consequences.

Consider a symmetric *static* scatterer in 1D with no potential gradient [Fig. 4 (a)]. Two identical wavepackets of momenta $\pm \hbar k$ simultaneously incident on opposite sides, should not give net current since scattering probabilities are independent of the side of incidence. That is indeed so if the scatterer is centered at the origin. But if it is shifted a distance d from the origin, we observe net flow, as shown in Fig. 1(c). The transport fraction $P = n_+ - n_-$ depends sinusoidally on the shift d , as shown in Fig. 3(a).

Classically impossible, such a current is a purely quantum effect due to coherent superposition of the left and right going packets; underscored by the fact that it is zero if the packets are incident *separately* as in Fig. 1(a) and (b), and then the resulting currents are added.

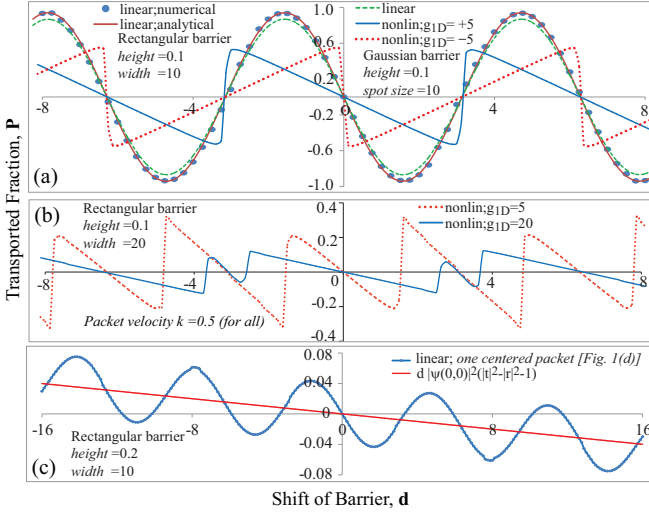


FIG. 3: Coherent transport by a shifted static barrier: (a) Two-wavepacket simulation [Fig. 1(c)] for rectangular barrier (dots) exactly matches analytical curve. Simulation with Gaussian barrier (laser profile) is close. Also shown are effects of (a) positive and negative nonlinearity g_{1D} and (b) different magnitudes of positive nonlinearity. (c) For a centered packet [Fig. 1(c)] small initial imbalance, due to barrier shift, tilts the net transport. Numerical curves are interpolations of points at intervals marked by the ‘dots’ in (a).

This can be understood by considering the scattering matrix elements [Fig. 4] of plane waves: $s_{12} = s_{21} = t$; $s_{11} = r e^{2ikd}$; $s_{22} = r e^{-2ikd}$. The transmission amplitudes are unaffected by the shift. But the reflection amplitudes undergo phase shifts, so the coherent sums on both sides, $\psi_{\pm}(x) = (t + r e^{\mp 2ikd}) e^{\pm ikx}$ give:

$$N = \frac{1}{2} [|\psi_+(x)|^2 + |\psi_-(x)|^2] = 1 + 2 \cos(2kd) \text{Re}\{t^* r\}$$

$$P = \frac{1}{2} [|\psi_+(x)|^2 - |\psi_-(x)|^2] = 2 \sin(2kd) \text{Im}\{t^* r\} \quad (5)$$

Number conservation requires $\text{Re}\{t^* r\} = 0$, but generally $\text{Im}\{t^* r\} \neq 0$ yielding non-vanishing P . Even with no shift, asymmetric scatterers can generate differential reflection phases, leading to net flow. This is demonstrated in Fig. 5, for the asymmetric double-barrier configuration of Fig. 4(b). While the transmission amplitudes are side-symmetric, the reflection amplitudes $S_{11(22)} = r_{l(r)} e^{-2ikd} + t_{l(r)}^2 r_{r(l)} e^{+2ikd} / (1 - r_r r_l e^{+4ikd})$ differ in phase unless the two barriers are identical.

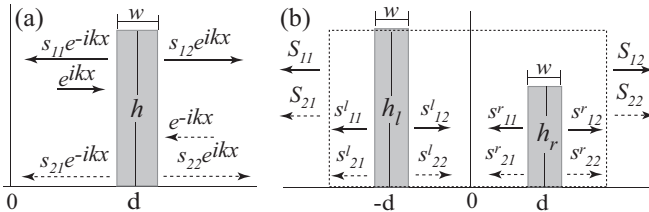


FIG. 4: Scattering matrix elements: (a) Single barrier shifted from the origin, (b) Double-barrier potential of separation $2d$.

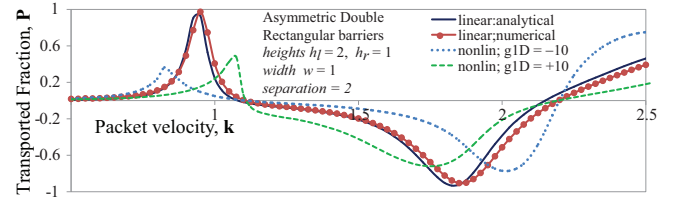


FIG. 5: Coherent transport by a static asymmetric double barrier potential: Wavepacket simulation for linear and nonlinear propagation; linear case matches analytical curve. Numerical plots are interpolations at intervals marked on one.

This effect is due to coherent superposition of the two waves $\pm k$ introducing a spatial periodicity that breaks translational invariance. Effect of bias is different, as can be seen with a packet initially centered at $x = 0$ [Fig 1(d)]. A barrier shift means more of the packet on one side. For $d \ll b$, this adds a term in Eq. (5): $P \simeq d|\psi(0,0)|^2(|t|^2 - |r|^2 - 1) + \sin(2kd) \text{Im}\{t^* r\}$ causing a linear tilt in P [Fig 3(c)]. Here, P is reduced by 1/2 as half of a centered packet is outbound.

Although non-classical, this is consistent with thermodynamics as there is no net current in a thermal mixture. Even for a 50-50 mixture of orthonormal states $\cos(kx)$ and $\sin(kx)$ the net current vanishes, as seen for the representative case of a shifted δ -potential $U\delta(x-d)$: $J[\cos(k)] = -J[\sin(k)] = -\sin(2kd) \hbar k^2 U / [2m(k^2 + U^2)]$.

Coherence in time-dependent phenomena: By running left and right going packets separately or simultaneously the role of quantum coherence in transport phenomena can be evaluated. We illustrate with two different time varying potentials associated with the mesoscopic process called quantum pumps [5]: (i) *snowplow*, where a single potential barrier [Fig. 4(a)] translates at uniform velocity $d = vt$ and (ii) *turnstile*, where heights of two barriers [Fig. 4(b)] vary out of phase, $h_l = h(1 + \sin(\omega t))$ and $h_r = h(1 + \cos(\omega t))$. For the snowplow, there is absolutely no difference in the current profile [Fig. 2] whether the two packets are run simultaneously or separately. This is because the shift d is now a function of time, so the sinusoidal dependence on the shift averages out. But, the turnstile pump shows a significant difference whether the left and right going packets interfere coherently or not, as seen in Fig. 6(a). This supports our earlier conclusions [5] that the snowplow pump can be simulated classically, but turnstile pumps involve quantum interference.

Effects of Interactions: Even a small interaction-induced nonlinearity can lead to a dramatic change of the transport features. As shown in Fig. 3 the dependence of the transport fraction P on the shift d changes from a sinusoidal to a triangular pattern, with sharp changes at specific values of the shift. Plots for small positive and negative nonlinearities are mirror images of each other across the anti-nodal planes of the sinusoidal curves for the corresponding linear case [Fig. 3(a)]. Even for the

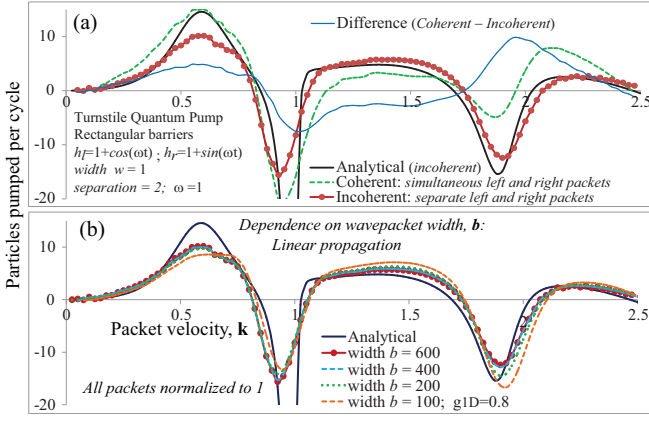


FIG. 6: Wavepacket simulation of a turnstile pump: (a) Coherent and incoherent transport compared to analytical results [3]. (b) Convergence with packet width ($b = 400$ and 600 indistinguishable); our estimates for ^{39}K correspond to $b = 100$, the small nonlinearity has no perceptible effect. *Plots are interpolations of points at intervals marked on one.*

asymmetric barriers [Fig. 5], nonlinearity sharpens the drop-off of the first peak. Since the superposition principle does not apply for nonlinear equations, general analytical solutions may not be possible, even with stationary solutions on hand [13]. Therefore, our method can be a valuable tool for probing nonlinear scattering and transport, by enabling direct comparison of numerical simulations and experiments in the same framework.

Nonlinear propagation is sensitive to the packet shape since the nonlinear term in the GP equation depends on $|\psi|^2$ which is non-uniform for a wavepacket, unlike for a plane wave. Therefore, rather than fix the normalization $\int dx |\psi(x, t)|^2$ as we vary the packet widths (as done in the linear case), we fix the product $g_{1D}|\psi(0, 0)|^2$, where $|\psi(0, 0)|^2$ is the initial peak density. This leads to consistent convergence with the nodes and the turning points occurring at convergent values, shown in Fig. 7. This does not happen if $\int dx |\psi(x, t)|^2$ is fixed instead. Note our nonlinearity $g_{1D}|\psi(0, 0)|^2 \sim 0.02$ is small enough to be in a regime where GP approximation is valid [14].

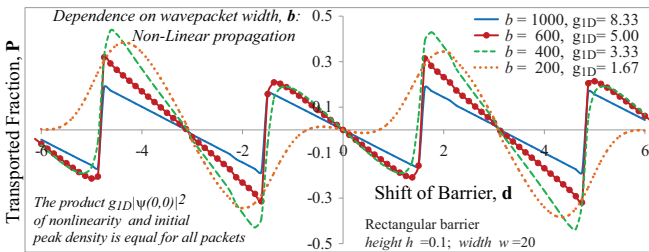


FIG. 7: Convergence with packet width for wavepacket simulation of nonlinear transport, keeping $g_{1D}|\psi(0, 0)|^2$ fixed; shown for coherent transport due to a shifted barrier. *Plots are interpolations of points at intervals marked on one.*

Conclusions and Outlook: We have presented an experimentally feasible and theoretically accurate way to conduct mesoscopic transport experiments relevant in solid state nanocircuits, with ultracold atoms. The tunability of parameters and absence of Coulomb interaction will allow study of transport phenomena with much broader possibilities. Coherence effects inherently suppressed in solid state systems can be made manifest with single mode transport studies possible with atoms. The predictable and sensitive coherent transfer due to small barrier shifts and asymmetries suggests applications for sensitive atom interferometers [15, 16] where the device laser is connected to a sensor; this can be quite robust since it measures scattered densities well separated in position and momentum space, without multi-step splitting-recombination of wavefronts, typical of interference effects as in Mach-Zehnder interferometers [16].

Nonlinearity in quantum coherent transport and scattering has very rich behavior as our simulations indicate. Our approach provides a simple numerical way, and a viable experimental method for probing such effects, still largely unexplored. Sharper variations with nonlinearity, as in Fig. 3, suggest that small interactions could actually be used to enhance interferometric sensitivity.

This work was funded by an NSF grant PHY-0970012. We thank S. Aubin and T. Opatrny for useful discussions.

-
- [1] A. Micheli *et al.*, Phys. Rev. Lett. **93**, 140408 (2004).
 - [2] R. A. Pepino *et al.*, Phys. Rev. Lett. **103**, 140405 (2009).
 - [3] B. T. Seaman *et al.*, Phys. Rev. A **75**, 023615 (2007).
 - [4] D. Ferry, S. M. Goodnick, and J. Bird, *Transport in Nanostructures* (Cambridge, USA, 2009), 2nd ed.
 - [5] K. K. Das and S. Aubin, Phys. Rev. Lett. **103**, 123007 (2009).
 - [6] R. Landauer, Phil. Mag. **21**, 863 (1970).
 - [7] J. Stenger *et al.*, Phys. Rev. Lett. **82**, 4569 (1999).
 - [8] C. Chin, R. Grimm, P. Julienne, and E. Tiesinga, Rev. Mod. Phys. **82**, 1225 (2010).
 - [9] R. Grimm, M. Weidemüller, and Y. B. Ovchinnikov, Adv. At. Mol. Opt. Phys. **42**, 95 (2000).
 - [10] K. K. Das, M. D. Girardeau, and E. M. Wright, Phys. Rev. Lett. **89**, 110402 (2002).
 - [11] G. Roati *et al.*, Phys. Rev. Lett. **99**, 010403 (2007).
 - [12] K. K. Das, Phys. Rev. A **66**, 053612 (2002); K. K. Das and T. Opatrny, Phys. Lett. A **374**, 485 (2010).
 - [13] T. Paul *et al.*, Phys. Rev. A **76**, 063605 (2007).
 - [14] T. Ernst, T. Paul, and P. Schlagheck, Phys. Rev. A **81**, 013631 (2010).
 - [15] P. R. Berman (editor), *Atom Interferometry* (Academic Press, USA, 1997).
 - [16] A. D. Cronin, J. Schmiedmayer, and D. E. Pritchard, Rev. Mod. Phys. **81**, 1051 (2009).